



Since January 2020 Elsevier has created a COVID-19 resource centre with free information in English and Mandarin on the novel coronavirus COVID-19. The COVID-19 resource centre is hosted on Elsevier Connect, the company's public news and information website.

Elsevier hereby grants permission to make all its COVID-19-related research that is available on the COVID-19 resource centre - including this research content - immediately available in PubMed Central and other publicly funded repositories, such as the WHO COVID database with rights for unrestricted research re-use and analyses in any form or by any means with acknowledgement of the original source. These permissions are granted for free by Elsevier for as long as the COVID-19 resource centre remains active.



Graphene oxide-graphene Van der Waals heterostructure transistor biosensor for SARS-CoV-2 protein detection

Jianwei Gao^{a,1}, Chunhua Wang^{a,1}, Yujin Chu^{a,1}, Yingkuan Han^a, Yakun Gao^a, Yanhao Wang^a, Chao Wang^a, Hong Liu^b, Lin Han^{a,**}, Yu Zhang^{a,*}

^a Institute of Marine Science and Technology, Shandong University, Qingdao, 266237, China

^b State Key Laboratory of Crystal Materials, Shandong University, Jinan, Shandong, 250100, China

ARTICLE INFO

Keywords:

Van der waals heterostructure
SARS-CoV-2
Protein detection
Graphene field-effect transistor

ABSTRACT

The current outbreaking of the coronavirus SARS-CoV-2 pandemic threatens global health and has caused serious concern. Currently there is no specific drug against SARS-CoV-2, therefore, a fast and accurate diagnosis method is an urgent need for the diagnosis, timely treatment and infection control of COVID-19 pandemic. In this work, we developed a field effect transistor (FET) biosensor based on graphene oxide-graphene (GO/Gr) van der Waals heterostructure for selective and ultrasensitive SARS-CoV-2 proteins detection. The GO/Gr van der Waals heterostructure was in-situ formed in the microfluidic channel through π - π stacking. The developed biosensor is capable of SARS-CoV-2 proteins detection within 20 min in the large dynamic range from 10 fg/mL to 100 pg/mL with the limit of detection of as low as \sim 8 fg/mL, which shows \sim 3 \times sensitivity enhancement compared with Gr-FET biosensor. The performance enhancement mechanism was studied based on the transistor-based biosensing theory and experimental results, which is mainly attributed to the enhanced SARS-CoV-2 capture antibody immobilization density due to the introduction of the GO layer on the graphene surface. The spiked SARS-CoV-2 protein samples in throat swab buffer solution were tested to confirm the practical application of the biosensor for SARS-CoV-2 proteins detection. The results indicated that the developed GO/Gr van der Waals heterostructure FET biosensor has strong selectivity and high sensitivity, providing a potential method for SARS-CoV-2 fast and accurate detection.

1. Introduction

COVID-19 is a newly emerged infectious disease associated with severe respiratory distress. Currently, there is no specific medicine for COVID-19 treatment. Early diagnosis and treatment are essential to control the epidemic. Diagnosing COVID-19 based on clinical symptoms is very difficult, especially in the early stages of the COVID-19, because there is no characteristic initial manifestation of COVID-19 [1–4]. Reliable laboratory diagnosis has become one of the primary tasks of epidemic prevention and control. In the detection of SARS-CoV-2 infections, reverse transcription-polymerase chain reaction (RT-PCR) is a commonly used method to specifically and sensitively detect virus RNA, which relies on complex instruments, skilled personnel and long-time

detection [5–8]. In particular, some areas with COVID-19 outbreaks usually do not have sufficient infrastructure to provide good RT-PCR diagnostic services. Therefore, it is essentially necessary to screen suspicious patients through another reliable diagnostic system. To diagnosis the COVID-19 rapidly and accurately, a few approaches were developed for detection of the RNA [9,10], Protein [11–13] and virus particles [14,15], including CRISPR-systems [16,17], surface enhanced Raman spectroscopy [18–20], microfluidic integrated biochip [21,22], electrochemical biosensors [23,24], and field-effect transistor (FET) based biosensors [25]. Among the existing diagnostic methods, the FET based biosensor delivers several obvious advantages for virus detection, including high selectivity through modified with target receptors, high sensitivity with label free process, real time electrical signal in-situ

* Corresponding author.

** Corresponding author.

E-mail addresses: gaoxiii@foxmail.com (J. Gao), hua52525252@163.com (C. Wang), chuyujin12306@163.com (Y. Chu), yingkuan.han@foxmail.com (Y. Han), 17854262215@163.com (Y. Gao), wangyanhao00@126.com (Y. Wang), 980606701@qq.com (C. Wang), hongliu@sdu.edu.cn (H. Liu), hanlin@sdu.edu.cn (L. Han), yuzhang@sdu.edu.cn (Y. Zhang).

¹ Authors contributed equally to this work.

<https://doi.org/10.1016/j.talanta.2021.123197>

Received 26 October 2021; Received in revised form 27 December 2021; Accepted 29 December 2021

Available online 31 December 2021

0039-9140/© 2021 Elsevier B.V. All rights reserved.

amplification and recording, cost-effective mass production with microelectronics manufacturing processes, and small size for portable point-of-care test [26–28]. Graphene, a one atom-thick large area 2D carbon material, has excellent chemical and physical properties in bio-sensing, such as good biocompatibility, strong interaction with biomolecules through π - π stacking and high intrinsic carrier mobility [29–31]. Many efforts have recently been devoted to the Gr-FET biosensors for highly sensitive and label-free cancer and virus protein detection [25,32,33]. The key is to improve the sensitivity and stability of the Gr-FET biosensors for the practical applications widely, as well as the understanding of sensing mechanisms. The channel surface modification or functionalization, such as graphene patterning [34], surface plasma pretreatment [35], Au nanoparticles [36], 1-pyrenebutyric acid succinimidyl ester (PBASE) [37], lipid membrane [38], PEG [39] and aptamers [40] etc., was studied to improve the sensitivity and stability of Gr-FET based biosensors for different biomarkers detection. The molybdenum disulfide/graphene nanostructure-based field-effect transistor biosensor was constructed and studied for sensitive RNA detection with donor effect dominated mechanism [41]. However, there is no any reports using graphene oxide/graphene van der Waals heterostructure FET biosensor for SARS-CoV-2 protein detection.

In this paper, we newly developed a graphene oxide-graphene van der Waals heterostructure FET biosensor integrated with microfluidic chip for label-free detection of SARS-CoV-2 protein with high sensitivity and specificity. The construction and performances of the Graphene oxide-graphene van der Waals heterostructure FET biosensor were studied comprehensively. The sensing performances enhancement mechanism was discussed based on the transistor-based biosensing theory and experimental results. Finally, the spiked SARS-CoV-2 protein samples in throat swab buffer solution were tested to confirm the practical application for COVID-19 protein detection. The ultrasensitive graphene oxide-graphene van der Waals heterostructure FET based biosensor will provide an alternative, portable strategy in diseases diagnosis and human health monitoring applications.

2. Experimental procedure

2.1. Materials

BSA, spike protein and nucleoprotein of SARS-CoV-2 were purchased from Sangon Biotech Company. Ethanolamine, Acetone, ferric chloride and isopropyl alcohol were purchased from Sinopharm. PBS was ordered from Corning. Polymethyl methacrylate (PMMA) was purchased from ALLRESIST, Germany. GO was prepared through a modified Hummers' method [42] Monolayer graphene film was grown using CVD on copper foil sheets (25 μm 99.8% purity) [43,44].

2.2. GO/Gr FET biosensor construction

The fabrication schematic of the biosensor is shown in Figure S1. Briefly, a single layer of graphene copper foil was protected with a thin PMMA layer; the copper foil sheet was etched away by 0.1 M FeCl_3 solution. The graphene was transferred onto a Si/SiO₂ substrate followed by PMMA removing using acetone. The 10 nm/50 nm Ti/Au source and drain electrodes were processed via the conventional microfabrication technology and electron beam evaporation deposition. A microfluidic chip was designed and fabricated using PDMS as the GO/Gr FET solution gate. A drop of GO solution was loaded into microfluidic channel and reacted with graphene for 1 h at room temperature to fully combine GO and graphene by π - π stacking interaction to form van der Waals heterostructure. An Ag/AgCl reference electrode and PBS solution were used as a gate electrode and gate solution, respectively. Fig. 1a shows the schematic structure of the biosensor.

2.3. Capture antibody immobilization and protein sensing

100 $\mu\text{g}/\text{mL}$ capture antibody was injected into the microfluidic channel and interacted for 1 h through π - π interaction with graphene oxide [22], followed by $1 \times$ PBS and DI water rinsing to remove the extra capture antibodies. Then the channel of the biosensor was blocked using

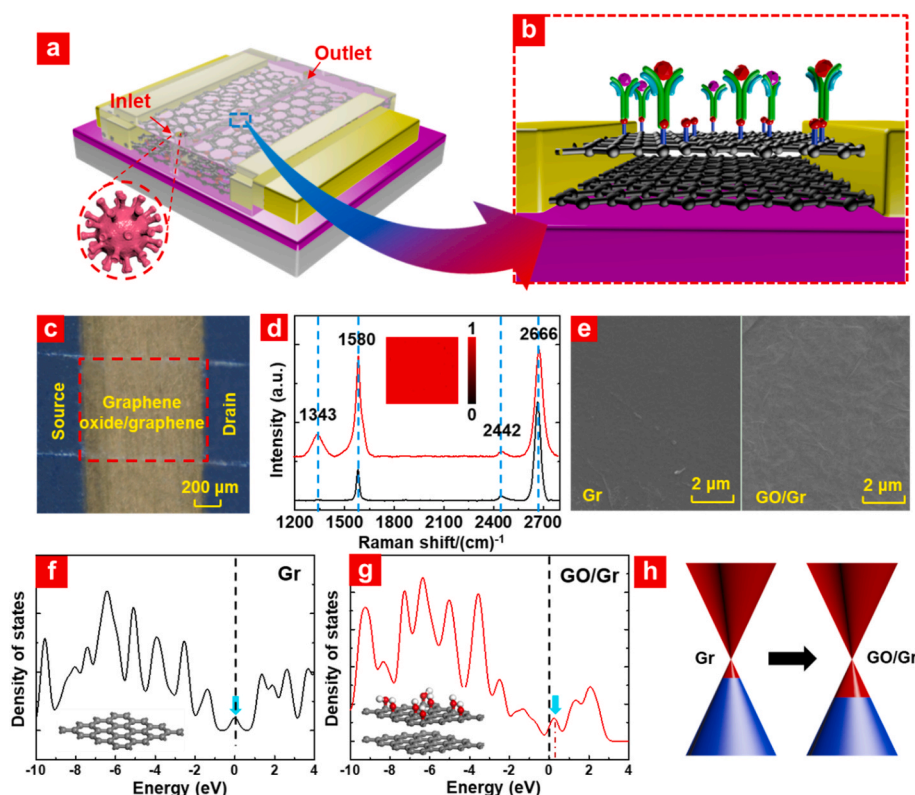


Fig. 1. (a) Schematic structure and (b) Spike protein detection illustration of the GO/Gr heterostructure FET biosensor. (c) Optical photo of the GO/Gr FET. (d) Raman spectra of the graphene (black) and graphene oxide/graphene (red). Inset shows spatial mapping of the Raman spectrum component analysis with graphene oxide/graphene over an area larger than $20 \mu\text{m} \times 20 \mu\text{m}$. (e) The SEM images of the transferred monolayer graphene and GO/Gr. Density of states from (f) monolayer graphene and (g) GO/Gr van der Waals heterostructure. (h) Schematic diagram of energy band structure for Gr and GO/Gr. (For interpretation of the references to colour in this figure legend, the reader is referred to the Web version of this article.)

BSA solution (100 mM, pH 9.0) for 30 min to eliminate possible nonspecific biomolecules adsorption followed by rinsing with $1 \times$ PBS. The capture antibody–protein reaction was performed by adding certain protein concentration solution into the device microfluidic channel and fully reacted with the immobilized capture antibody for 20 min. Finally, the biosensor microfluidic channel was flushed with $1 \times$ PBS. Fig. 1b illustrated the GO/Gr FET biosensor basic working mechanism for miRNA detection. The reaction of specific protein with capture antibody causes n-doping of the biosensor channel graphene [45,46].

2.4. Electrical characterization of GO/Gr FET

The SARS-CoV-2 proteins concentration dependent electrical response was characterized by recording the I–V curves on the probe station with a source meter Keithley 2636 B. Figure S1h shows the measurement circuit connection detail of the device. For the I_{ds} – V_{ds} curves, the sweep range of V_{ds} was set from -50 mV to 50 mV with increments of 0.1 V. For the I_{ds} – V_{gs} curves, the sweep range of V_{gs} was set from -200 mV to 300 mV at a fixed V_{ds} of 50 mV.

3. Results and discussion

3.1. The GO/Gr heterostructure characterization

Fig. 1c shows the optical image of the manufactured GO/Gr FET, where the GO/Gr sheet passes fully cross the source and drain form channel (the red dotted rectangle). The GO nanosheets were stacked on the graphene surface through π – π stacking to form a GO/Gr heterostructure. To confirm the GO/Gr heterostructure, Raman spectra of monolayer graphene with and without GO stacking are characterized. The 2D peak to G peak ratio is 2.8 for the graphene (Fig. 1d), indicating the transferred graphene is the monolayer graphene. After the formation of the GO/Gr heterostructure, it can be clearly observed the characteristic peaks of GO ($1343, 1580$ cm^{-1}) with decreased 2D peak to G peak ratio (~ 1), as shown in Fig. 1d (red line). The heating mapping shows that the graphene oxide nanosheets are uniformly distributed on the graphene (inset of Fig. 1d). Fig. 1e shows the graphene scanning electron microscopy (SEM) images with and without of GO. The transferred monolayer graphene is relative flat without wrinkles, GO/Gr shows a little bit rough surface due to the GO nanosheets.

In order to further confirm the GO/Gr heterostructure, density functional theory (DFT) calculations were performed with Materials studio using the Castep simulation package to investigate the Density of State (DOS) of the graphene and GO/Gr heterostructure (Fig. 1f–g). The simulation results show that the band gap of graphene is opened and the carrier mobility of the GO/Gr is improved due to the interaction of graphene and GO after the formation of the GO/Gr van der Waals heterojunction. GO can form covalent bonds with carbon atoms in graphene, which results in the transformation of hybridization from sp^2 to sp^3 , causing to bandgap opening [47]. The GO with abundant $-OH$ groups can transfer charge to graphene. The strong electronic coupling between GO as an electron donor and graphene as an electron acceptor leads to charges in the van der Waals heterojunction redistribution at the interface resulting in the p-doping of the graphene (Fig. 1h). DFT calculations further confirmed the formation of a GO/Gr heterojunction, and thereby gave hint to increase the sensitivity of biomolecules detection.

3.2. The GO/Gr FET biosensor electrical performances

Under a constant V_{gs} , the output curves of the Gr FET and GO/Gr FET show linear properties (Fig. 2a). After the formation of GO/Gr heterojunction, the device resistance increases due to the interaction between nonconductive GO and graphene. In Figure S2, the ambipolar behaviors of both GO/Gr and Gr FETs are obtained, and Dirac point V_{Dirac} of the GO/Gr FET shifts right to ~ 119 mV from ~ 75 mV of the Gr FET, which is consistent with the simulation results shown in Fig. 1f–g. The V_{Dirac} right shift indicates that the graphene is p-doped after GO stack on the graphene through π – π stacking [48,49]. The mobility of GO/Gr heterojunction FET is increased by about 1.5 times comparing to the Gr FET, which greatly improves the performance of the device due to the effective patch of the graphene detects and suppression of surface ions absorption [50,51]. GO forms a uniform protective layer on the surface of graphene, which can prevent the direct contact of external ions with the surface of graphene, plays the role of protective layer and prevents the influence of external ions on the mobility of graphene. At the same time, due to the formation of heterojunction, the electron exchange efficiency is improved through interface coupling, and the mobility of the device is further improved [52]. After capture protein antibody immobilization, the V_{Dirac} of both Gr FET and GO/Gr FET biosensor shifted to

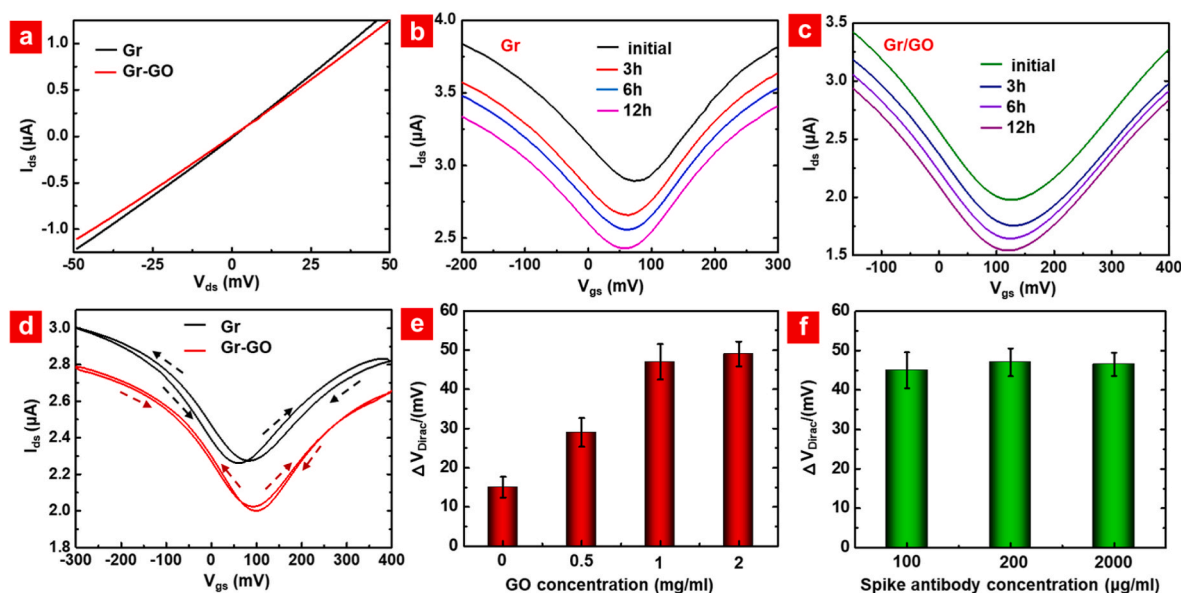


Fig. 2. (a) The output curves of the GO/Gr heterostructure FET and Gr-FET at $V_{gs} = 0$. The time dependent transfer curves of (b) the Gr FET and (c) the GO/Gr heterostructure FET at $V_{ds} = 50$ mV (d) Hysteresis curve of the GO/Gr heterostructure FET and Gr-FET at $V_{ds} = 50$ mV. (e) The GO concentrations dependent ΔV_{Dirac} of the GO/Gr heterostructure FET biosensor. (f) Capture antibody concentrations dependent ΔV_{Dirac} of the GO/Gr heterostructure FET biosensor.

left due to capture antibody and protein induced graphene channel n-doping (Figure S2b-c). To evaluate the stability of the devices in solution, we tested the time dependent electrical properties of the devices in $1 \times$ PBS solution. As shown in Fig. 2b-c, the V_{Dirac} shift of GO/Gr FET is only less than 5 mV comparing to the Gr-FET of 12–19 mV after 12 h storage in PBS solution, which shows the improved stability after the formation of heterojunction due to making up for the lattice defects of graphene and effective protection layer of GO in the solution. The possible reason of the V_{Dirac} shift is due to the interaction between the device and the ions in PBS solution, and the Dirac point shifts of the GO/Gr FET and Gr FET are comparable with the previous reports and acceptable in real applications [53]. To further confirm the stability of the GO/Gr and Gr FETs, we performed the hysteresis test since the Gr FET normally exhibits hysteresis due to water absorption on the channel surface when it works as biosensors [54]. As shown in Fig. 2d, the GO/Gr FET presents ~ 3 times smaller V_{Dirac} shift of ~ 11 mV comparing to Gr FET with ~ 29 mV V_{Dirac} shift. It further confirms that the formation of GO/Gr heterojunction increases the stability of the GO/Gr FET. The resistance increases due to the adsorption of ions in the liquid gate dielectric layer on the surface of graphene, and causes the increase of charge impurity scattering [55].

To construct the best GO/Gr heterostructure, we optimized the GO concentrations by adding 0.5 mg/mL, 1 mg/mL, and 2 mg/mL GO on the surface of graphene and incubating at room temperature for 1 h. After the GO/Gr van der Waals heterostructure formed, The 100 $\mu\text{g/mL}$ antibody was fixed on the GO/Gr FET channel surface, and the 100 pg/mL antigen was added to detect the sensor response. As shown in the Fig. 2e, the V_{Dirac} shift of the GO/Gr van der Waals heterostructure biosensor formed by 1 mg/mL GO reached the maximum. Here, the absolute value of Dirac point shift was represented by ΔV_{Dirac} . Therefore, 1 mg/mL was chosen as the optimal GO concentration for the GO/Gr van der Waals heterostructure biosensor construction. In order to capture the antigen, the antibody is required to achieve saturated adsorption on the surface of the biosensors. We incubate 100 $\mu\text{g/mL}$, 200 $\mu\text{g/mL}$ and 2000 $\mu\text{g/mL}$ antibodies on the graphene surface for 1 h at room temperature. Then, 100 pg/mL antigen was added to detect the sensor response. When the antibody concentration increased from 100 to 2000 $\mu\text{g/mL}$, the Dirac point shift of the biosensor just showed slightly

increase, indicating that the 100 $\mu\text{g/mL}$ antibody could be fully immobilized on the GO/Gr FET biosensor channel surface. Therefore, 100 $\mu\text{g/mL}$ antibody is preferred as the optimal antibody incubation concentration.

3.3. The SARS-CoV-2 protein detection of the GO/Gr FET biosensor

To test the sensitivity of the GO/Gr FET biosensor for the SARS-CoV-2 protein detection, SARS-CoV-2 spike protein was diluted into different concentrations from 10 fg/mL to 100 pg/mL and applied to the GO/Gr FET biosensor channel. In Fig. 3a, the V_{Dirac} of the GO/Gr FET biosensor shifted toward left with increased concentrations of the specific spike protein from 10 fg/mL to 100 pg/mL. As a comparison, we also tested the sensitivity of Gr FET biosensor for the SARS-CoV-2 spike protein from 10 fg/mL to 100 pg/mL. V_{Dirac} shows similar response to specific spike protein concentration but smaller shift values, as shown in Fig. 3b. Fig. 3c shows a linear relationship between spike protein concentrations and changes of the Dirac point for both biosensors. The GO/Gr FET biosensor presents a sensitivity of 12.8 mV/decade with correlation coefficient $R^2 = 0.98249$, while the sensitivity of Gr-FET degraded to 4.76 mV/decade. The blue dash line represents the noise level, which was the Dirac point shift value obtained by completely fixing the antibody protein on the surface of graphene, blocking it with BSA buffer and adding PBS buffer for transfer characteristic curves. We have also done two repeatability experiments of SARS-CoV-2 Spike protein detection by using different batches of GO/Gr FET biosensors. The average sensitivity is 11.68 mV/decade (Figure S3). We also used GO/Gr heterostructure biosensor to detect SARS-CoV-2 nucleoprotein. The similar results were obtained with the sensitivity of 11.19 mV/decade (Figure S4). All the results showed that the GO/Gr heterostructure FET biosensor improved the SARS-CoV-2 protein detection sensitivity by a factor of ~ 3 . The slight difference in detection sensitivity is due to the quality and process variation of the graphene in different devices.

To study the specificity of the GO/Gr FET biosensor, the same concentration of the proteins (AFP, SARS-CoV-2 spike protein and SARS-CoV-2 nucleoprotein) was interacted with the SARS-CoV-2 spike protein capture antibody and the SARS-CoV-2 nucleoprotein capture antibody in the channel of GO/Gr FET biosensor, respectively. Another two

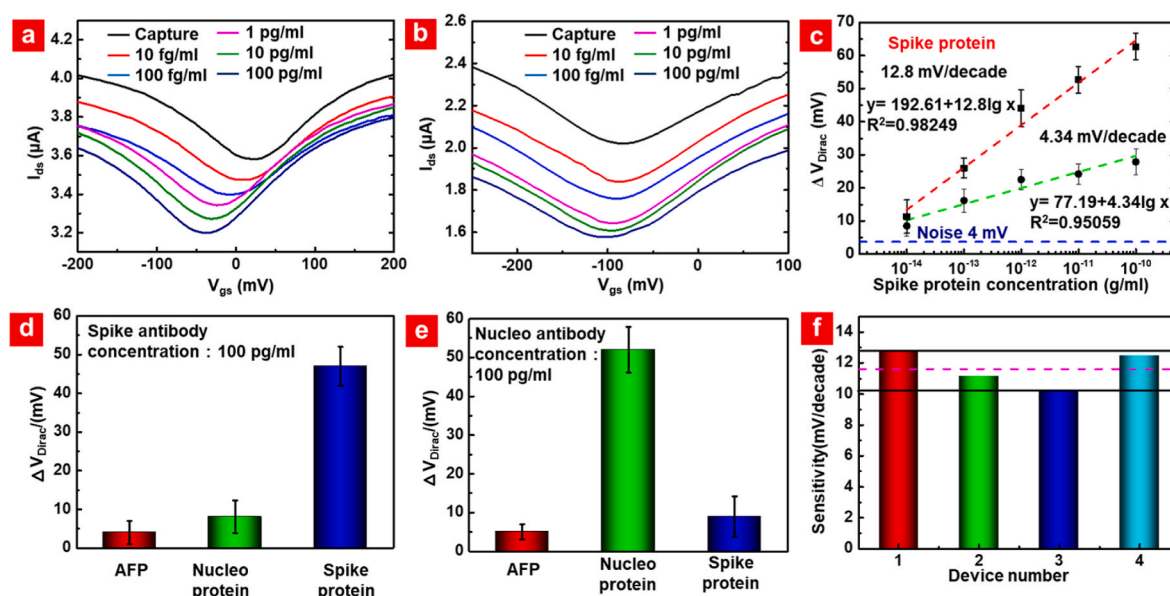


Fig. 3. The SARS-CoV-2 spike protein concentrations dependent transfer curves of (a) GO/Gr FET biosensor and (b) Gr FET biosensor. (c) The SARS-CoV-2 spike protein concentrations dependent ΔV_{Dirac} shifts for both GO/Gr FET (red line) and Gr FET (green line) biosensors. The ΔV_{Dirac} shift of the GO/Gr FET biosensor with (d) SARS-CoV-2 spike protein capture antibody and (e) SARS-CoV-2 nucleoprotein capture antibody for 100 pg/mL AFP, SARS-CoV-2 nucleoprotein and SARS-CoV-2 spike protein detection. (f) The sensitivity from the different batches of GO/Gr FET biosensors. (For interpretation of the references to colour in this figure legend, the reader is referred to the Web version of this article.)

proteins are used as non-target proteins. The V_{Dirac} of the GO/Gr FET biosensor shifts to the left 49 mV after adding 100 $\mu\text{g}/\text{mL}$ spike protein. The V_{Dirac} just shows slightly shift after loading non-target proteins, which are 4 and 9 mV shift to the left for AFP and nucleoprotein, respectively, as shown in Fig. 3d. At the same time, we also tested the specificity of the GO/Gr FET biosensor to the SARS-CoV-2 nucleoprotein, and the results showed that it also has a very good specificity for the nucleoprotein, as shown in Fig. 3e. Therefore, we could conclude that the GO/Gr van der Waals heterostructure FET biosensor shows good selectivity for SARS-CoV-2 protein detection. To evaluate the detection stability, the SARS-CoV-2 protein detection was performed by using different batches of GO/Gr FET biosensors. The sensitivity of different GO/Gr FET biosensors are shown in Fig. 3f. The average sensitivity value of the GO/Gr FET biosensors is 11.69 mV/decade with the standard deviation of 10.25%, which proves the relatively stable detection performance from different batches of GO/Gr FET biosensors.

3.4. The sensing mechanisms of the GO/Gr FET biosensor

GO with abundant functional groups (OH-, COOH-, CO-) has an improved adsorption force for target molecules than graphene [56,57]. Firstly, we studied the SARS-CoV-2 capture antibody adsorption density of the GO/Gr FET and Gr-FET biosensors based on indirect manner-fluorescence detection (Elisa principle [22,58]), and direct manner-Raman detection. The schematic diagram of fluorescence detection is shown in Figure S4a and S5, and the Raman detection is shown in Figure S6. The SARS-CoV-2 capture antibody of the 100 $\mu\text{g}/\text{mL}$ was firstly immobilized on the GO/Gr FET and Gr-FET biosensor channel surface through the microfluidic. Then the SARS-CoV-2 spike protein of 100 $\mu\text{g}/\text{mL}$ was incubated in the GO/Gr FET and Gr-FET biosensors channel for 20 min, respectively. After that the Cy5-streptavidin-biotinylated SARS-CoV-2 detection antibody was added to react with protein for 20 min. The scanned fluorescence signals were obtained by Genepix 4400 after rinse and dry. Fig. 4b shows the detection fluorescence results. The fluorescence intensity on the surface of the GO/Gr FET biosensor is ~ 3.6 times higher than that of the Gr-FET biosensor, meaning that more capture antibody immobilization and higher SARS-CoV-2 antibody and protein reaction efficiency on the GO/Gr FET biosensor. The Raman signal in Figure S6 also shows higher

representative peak intensity on GO/Gr device than that on Gr device, indicating more capture antibody immobilization on GO/Gr device. We reasoned that the abundant functional groups of GO nanosheets reacted strongly with SARS-CoV-2 capture antibodies via both π - π stacking and hydrogen bonding [59] resulting in the improved detection sensitivity of the GO/Gr FET biosensors.

For the electrical FET biosensor, applying a gate voltage V_{gs} in the gate solution will result in the formation of an electric double layer (EDL) at the polarizable electrode/electrolyte interface. As shown in Fig. 4c. When the SARS-CoV-2 spike protein reaction with the capture antibody, the charge (Δq) changed at the solution-graphene interface, which results in changing the electrostatic potential in the channel and causes the Dirac point to shift followed by the equation [37]:

$$\Delta V_{Dirac} = \frac{\Delta q}{C} \quad (2)$$

Where c is the total gate capacitance (C) of the GO/Gr FET biosensor. As we can see that there are more charged SARS-CoV-2 spike proteins capture antibody on the surface of the GO/Gr heterojunction, it would enhance the protein and capture antibody reaction efficiency, thus, causing a more obvious Dirac point shift for the GO/Gr FET biosensor compared to the Gr-FET biosensor.

The Debye length, typically less than 1 nm in physiological conditions [60,61], is also particularly important for the FET biosensor due to the charge screening effect. Generally, the antibody (~ 5 –20 nm in size) and protein (~ 5 –10 nm in size) molecules are larger than the nucleic acid molecules, which results in lower sensitivity due to the strong charge screening [62]. Therefore, breaking or beyond the Debye screening limit to obtain high performance field effect based biosensor is a major challenge [61]. In this work, GO nanosheets were functionalized on the Gr FET, and the SARS-CoV-2 spike antibody and protein reaction occurred over the GO, and the sensing performance of the GO/Gr FET biosensor was improved. Does the GO functionalization on the Gr FET influence the Debye length? To answer the question, we studied the V_{Dirac} shift behaviors of the GO/Gr FET and Gr FET biosensors with the same SARS-CoV-2 spike protein concentration (100 $\mu\text{g}/\text{mL}$) under different ionic strengths. Fig. 4d shows the detected results of 100 $\mu\text{g}/\text{mL}$ SARS-CoV-2 spike protein using the GO/Gr FET and Gr FET biosensors and theoretical Debye length under $0.1 \times$, $0.5 \times$, $1 \times$, $5 \times$,

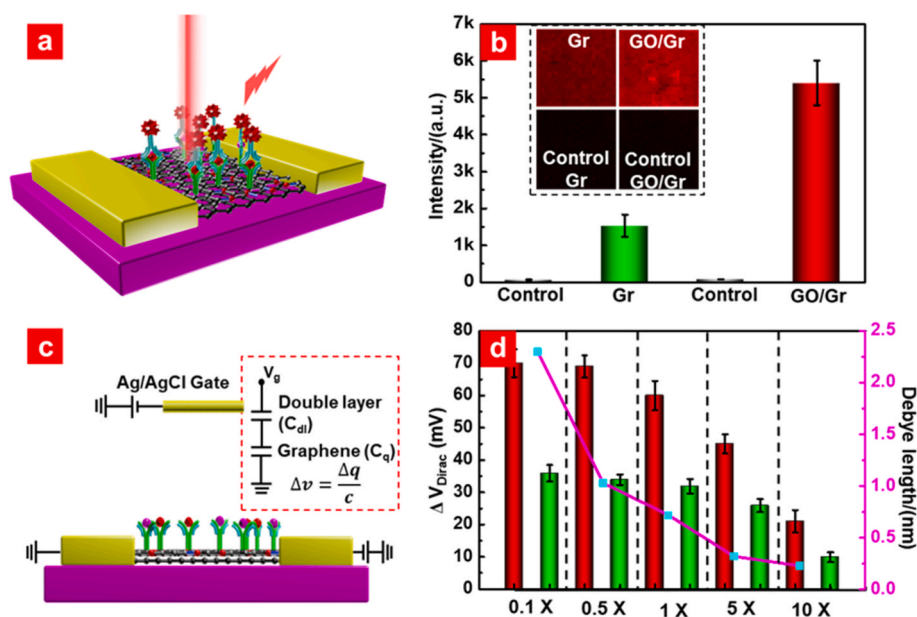


Fig. 4. (a) Mechanism verification schematic of the GO/Gr and Gr FET biosensors by ELISA fluorescence method. (b) Fluorescence signal of APC after 100 $\mu\text{g}/\text{mL}$ SARS-CoV-2 antigen on Gr and GO/Gr. Inset: the scanned fluorescence mapping patterns on Gr and GO/Gr. (c) Schematic diagram of electric double layer model of biosensor. (d) Comparison of Dirac point change of GO/Gr FET and Gr FET biosensors in different PBS concentrations.

and $10 \times$ PBS buffer solutions. The V_{Dirac} shifts of both the GO/Gr FET biosensor are larger than that of the Gr-FET biosensor at all PBS concentrations. The Dirac point shifts of both the GO/Gr FET and Gr-FET biosensors increase with the decrease of PBS concentration at high PBS concentrations ($1 \times \sim 10 \times$) due to the correlation between the ionic strength and the EDL capacitance in the electrolyte-gating system [38]. However, The Dirac point shift gets saturation with further decrease PBS concentration to $0.1 \times$ and $0.5 \times$ for both the GO/Gr FET and Gr-FET biosensors. It means that the target analytes get into the domain of Debye length and the charge effect on the biosensor reaches maximum at the PBS concentration below $0.5 \times$ for both GO/Gr FET and Gr FET biosensors. The electrification of protein is caused by its carboxyl, hydroxyl and other charged groups. These groups are on the surface of the protein. Although Debye shielding will shield the charges outside the Debye radius, signal can also be detected [63]. It's obviously that the Gr FET biosensor without any functionalization cannot change the Debye length of the detection system. Therefore, the performance enhancement of the GO/Gr FET biosensor could not be attributed to the Debye length increase, which mainly benefits from the improved capture antibody immobilization density.

3.5. The practical application of the GO/Gr FET biosensor

To verify the practical application ability of the GO/Gr FET biosensor in actual samples, we took throat swabs from healthy people and spiked the SARS-CoV-2 spike protein and nucleoprotein in it since the actual SARS-CoV-2 test is performed using those method. Firstly, we took $1 \mu\text{L}$ 100 pg/mL spike protein and $1 \mu\text{L}$ 100 pg/mL nucleoprotein to mix with $8 \mu\text{L}$ healthy human throat swab buffer solution. Then the mixture samples and healthy human throat swab solution were tested at the same time to prove the actual sample detection capability of the GO/Gr FET biosensor. In Fig. 5, the GO/Gr FET biosensor V_{Dirac} shifts for spiked actual samples detection is much larger than that for healthy human samples detection, indicating that the GO/Gr FET biosensor can distinguish the protein levels in the throat swab solutions. The results proved that the GO/Gr FET biosensor could be as a label-free, fast, and sensitive tool for SARS-CoV-2 protein analysis.

4. Conclusion

In summary, we have developed the GO/Gr van der Waals heterostructure FET biosensor capable of achieving ultrasensitive, label-free, specific and fast detection of SARS-CoV-2 proteins. The GO/Gr van der Waals heterostructure was formed by stacking GO nanosheets on the monolayer graphene via π - π stacking. Compared to Gr FET biosensor, the $3 \times$ sensitivity enhancement of the GO/Gr heterostructure FET biosensor was achieved for SARS-CoV-2 protein detection. The sensing mechanisms of the developed GO/Gr heterostructure biosensor were studied simulatively and experimentally, which is attributed to the enhanced capture antibody immobilization density due to abundant functional groups on the GO. The detection of the spiked SARS-CoV-2 spike protein in healthy human throat swab solution proved the practical application potential for real COVID-19 protein analyzation.

Credit author statement

Yu Zhang and Lin Han designed the study and revised the manuscript; Jianwei Gao carried out the experiments and wrote this manuscript; Chunhua Wang carried out the fluorescence detection experiment, Yunjin Chu carried out the material energy band simulation. Yakun Gao assisted in the completion of the experiment; Yingkuan Han conducted graphene nanosheets characterization; Yanhao Wang and Chao Wang made microfluidic chips; Hong Liu performed theoretical analysis.

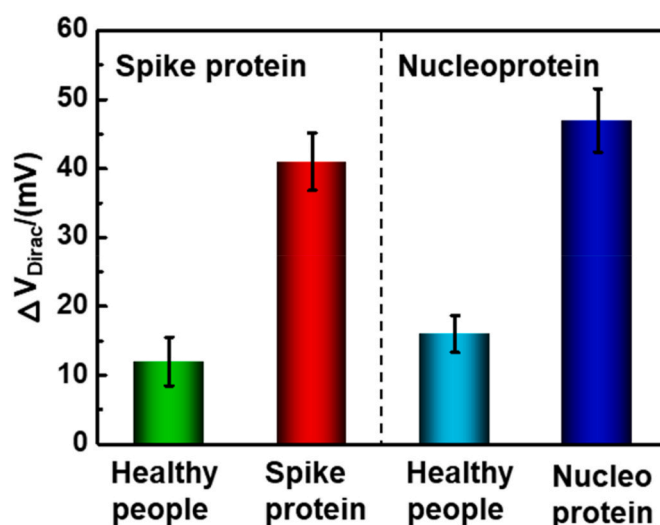


Fig. 5. The detection results of spiked SARS-CoV-2 proteins in healthy human throat swab solution by the GO/Gr FET biosensors.

Declaration of competing interest

The authors declare that they have no known competing financial interests or personal relationships that could have appeared to influence the work reported in this paper.

Acknowledgement

This work was supported by the National Key R&D Plan of China (Grant No. 2017YFB0405400), State Key Laboratory of Microbial Technology Open Projects Fund (Project NO. M2021-01 and M2021-07), Shandong University multidisciplinary research and innovation team of young scholars, Collaborative Innovation Center of Technology and Equipment for Biological Diagnosis and Therapy in Universities of Shandong. We would like to thank Haiyan Yu, Xiaomin Zhao, Sen Wang and Yuyu Guo from State Key laboratory of Microbial Technology of Shandong University for help and guidance in material characterization.

Appendix A. Supplementary data

Supplementary data to this article can be found online at <https://doi.org/10.1016/j.talanta.2021.123197>.

References

- [1] X. Cao, COVID-19: immunopathology and its implications for therapy, *Nat. Rev. Immunol.* 20 (2020) 269–270.
- [2] A. Nalbandian, K. Sehgal, A. Gupta, M.V. Madhavan, C. McGroder, J.S. Stevens, et al., Post-acute COVID-19 syndrome, *Nat. Med.* 27 (2021) 601–615.
- [3] M. Cevik, S.D. Baral, Networks of SARS-CoV-2 transmission, *Sci* 373 (2021) 162.
- [4] P.J. Hotez, C. Batista, Y.B. Amor, O. Ergonul, J.P. Figueroa, S. Gilbert, et al., Global public health security and justice for vaccines and therapeutics in the COVID-19 pandemic, *EclinicalMedicine* 39 (2021) 101053.
- [5] B.D. Kevadiya, J. Machhi, J. Herskovitz, M.D. Oleynikov, W.R. Blomberg, N. Bajwa, et al., Diagnostics for SARS-CoV-2 infections, *Nat. Mater.* 20 (2021) 593–605.
- [6] L. Mutesa, P. Ndishimye, Y. Butera, J. Souopgui, A. Uwineza, R. Rutayisire, et al., A pooled testing strategy for identifying SARS-CoV-2 at low prevalence, *Nature* 589 (2021) 276–280.
- [7] M.S. Han, J.-H. Byun, Y. Cho, J.H. Rim, RT-PCR for SARS-CoV-2: quantitative versus qualitative, *Lancet Infect. Dis.* 21 (2021) 165.
- [8] W. Feng, A.M. Newbigging, C. Le, B. Pang, H. Peng, Y. Cao, et al., Molecular diagnosis of COVID-19: challenges and research needs, *AnaChronist* 92 (2020) 10196–10209.
- [9] K. Razzini, M. Castrica, L. Menchetti, L. Maggi, L. Negroni, N.V. Orfeo, et al., SARS-CoV-2 RNA detection in the air and on surfaces in the COVID-19 ward of a hospital in Milan, Italy, *SciEn* 742 (2020) 140540.
- [10] T. Chaibun, J. Puenpa, T. Ngamdee, N. Boonapatcharoen, P. Athamanolap, A. P. O'Mullane, et al., Rapid electrochemical detection of coronavirus SARS-CoV-2, *Nat. Commun.* 12 (2021) 802.

- [11] K. Guo, S. Wustoni, A. Koklu, E. Díaz-Galicia, M. Moser, A. Hama, et al., Rapid single-molecule detection of COVID-19 and MERS antigens via nanobody-functionalized organic electrochemical transistors, *Nat. Biomed. Eng.* 5 (2021) 666–677.
- [12] S. Dispinseri, M. Secchi, M.F. Pirillo, M. Tolazzi, M. Borghi, C. Brigatti, et al., Neutralizing antibody responses to SARS-CoV-2 in symptomatic COVID-19 is persistent and critical for survival, *Nat. Commun.* 12 (2021) 2670.
- [13] A.M.M. Murillo, J. Tomé-Amat, Y. Ramírez, M. Garrido-Arandia, L.G. Valle, G. Hernández-Ramírez, et al., Developing an Optical Interferometric Detection Method based biosensor for detecting specific SARS-CoV-2 immunoglobulins in Serum and Saliva, and their corresponding ELISA correlation, *Sensor. Actuator. B Chem.* 345 (2021) 130394.
- [14] H. Yousefi, A. Mahmud, D. Chang, J. Das, S. Gomis, J.B. Chen, et al., Detection of SARS-CoV-2 viral particles using direct, reagent-free electrochemical sensing, *J. Am. Chem. Soc.* 143 (2021) 1722–1727.
- [15] H. Zhao, F. Liu, W. Xie, T.-C. Zhou, J. OuYang, L. Jin, et al., Ultrasensitive sandwich-type electrochemical sensor for SARS-CoV-2 from the infected COVID-19 patients using a smartphone, *Sensor. Actuator. B Chem.* 327 (2021) 128899.
- [16] H. Rahimi, M. Salehiabar, M. Barsbay, M. Ghaffarlou, T. Kavetskiy, A. Sharafi, et al., CRISPR systems for COVID-19 diagnosis, *ACS Sens.* 6 (2021) 1430–1445.
- [17] J.P. Broughton, X. Deng, G. Yu, C.L. Fasching, V. Servellita, J. Singh, et al., CRISPR-Cas12-based detection of SARS-CoV-2, *Nat. Biotechnol.* 38 (2020) 870–874.
- [18] Y. Yang, Y. Peng, C. Lin, L. Long, J. Hu, J. He, et al., Human ACE2-functionalized gold “virus-trap” nanostructures for accurate capture of SARS-CoV-2 and single-virus SERS detection, *Nano-Micro Lett.* 13 (2021) 109.
- [19] C. Wang, X. Cheng, L. Liu, X. Zhang, X. Yang, S. Zheng, et al., Ultrasensitive and simultaneous detection of two specific SARS-CoV-2 antigens in human specimens using direct/enrichment dual-mode fluorescence lateral flow immunoassay, *ACS Appl. Mater. Interfaces* 13 (2021) 40342–40353.
- [20] S. Chen, L. Meng, L. Wang, X. Huang, S. Ali, X. Chen, et al., SERS-based lateral flow immunoassay for sensitive and simultaneous detection of anti-SARS-CoV-2 IgM and IgG antibodies by using gap-enhanced Raman nanotags, *Sensor. Actuator. B Chem.* 348 (2021) 130706.
- [21] Y. Chu, Y. Gao, W. Tang, L. Qiang, Y. Han, J. Gao, et al., Attomolar-level ultrasensitive and multiplex microRNA detection enabled by a nanomaterial locally assembled microfluidic biochip for cancer diagnosis, *AnaChronist* 93 (2021) 5129–5136.
- [22] C. Wang, C. Wang, J. Qiu, J. Gao, H. Liu, Y. Zhang, et al., Ultrasensitive, high-throughput, and rapid simultaneous detection of SARS-CoV-2 antigens and IgG/IgM antibodies within 10 min through an immunoassay biochip, *Microchim. Acta* 188 (2021) 262.
- [23] M. Alafeef, K. Dighe, P. Moitra, D. Pan, Rapid, ultrasensitive, and quantitative detection of SARS-CoV-2 using antisense oligonucleotides directed electrochemical biosensor chip, *ACS Nano* 14 (2020) 17028–17045.
- [24] M.S. Kumar, R. Nandeshwar, S.B. Lad, K. Megha, M. Mangat, A. Butterworth, et al., Electrochemical sensing of SARS-CoV-2 amplicons with PCB electrodes, *Sensor. Actuator. B Chem.* 343 (2021) 130169.
- [25] G. Seo, G. Lee, M.J. Kim, S.-H. Baek, M. Choi, K.B. Ku, et al., Rapid detection of COVID-19 causative virus (SARS-CoV-2) in human nasopharyngeal swab specimens using field-effect transistor-based biosensor, *ACS Nano* 14 (2020) 5135–5142.
- [26] Y. Liang, M. Xiao, D. Wu, Y. Lin, L. Liu, J. He, et al., Wafer-scale uniform carbon nanotube transistors for ultrasensitive and label-free detection of disease biomarkers, *ACS Nano* 14 (2020) 8866–8874.
- [27] C.-R. Wu, S.-L. Wang, P.-H. Chen, Y.-L. Wang, Y.-R. Wang, J.-C. Chen, Demonstration of the enhancement of gate bias and ionic strength in electric-double-layer field-effect-transistor biosensors, *Sensor. Actuator. B Chem.* 334 (2021) 129567.
- [28] E. Danielson, V.A. Sontakke, A.J. Porkovich, Z. Wang, P. Kumar, Z. Ziadi, et al., Graphene based field-effect transistor biosensors functionalized using gas-phase synthesized gold nanoparticles, *Sensor. Actuator. B Chem.* 320 (2020) 128432.
- [29] K. Mensah, I. Cissé, A. Pierret, M. Rosticher, J. Palomo, P. Morfin, et al., DNA hybridization measured with graphene transistor arrays, *Adv. Healthcare Mater.* 9 (2020) 2000260.
- [30] T. Murugathas, C. Hamiaux, D. Colbert, A.V. Kralicek, N.O.V. Plank, C. Carraher, Evaluating insect odorant receptor display formats for biosensing using graphene field effect transistors, *ACS Appl. Elect. Mater.* 2 (2020) 3610–3617.
- [31] N. Yogeswaran, E.S. Hosseini, R. Dahiya, Graphene based low voltage field effect transistor coupled with biodegradable piezoelectric material based dynamic pressure sensor, *ACS Appl. Mater. Interfaces* 12 (2020) 54035–54040.
- [32] Y. Kanai, Y. Ohmuro-Matsuyama, M. Tanioku, S. Ushiba, T. Ono, K. Inoue, et al., Graphene field effect transistor-based immunosensor for ultrasensitive noncompetitive detection of small antigens, *ACS Sens.* 5 (2020) 24–28.
- [33] J. Gao, Y. Gao, Y. Han, J. Pang, C. Wang, Y. Wang, et al., Ultrasensitive Label-free miRNA Sensing Based on a Flexible Graphene Field-Effect Transistor without Functionalization, *ACS Applied Electronic Materials*, 2020.
- [34] S.S. Kwon, D. Kim, M. Yun, J.G. Son, S.H. Lee, The role of graphene patterning in field-effect transistor sensors to detect the tau protein for Alzheimer's disease: simplifying the immobilization process and improving the performance of graphene-based immunosensors, *Biosens. Bioelectron.* 192 (2021) 113519.
- [35] Q. Yuan, S. Wu, C. Ye, X. Liu, J. Gao, N. Cui, et al., Sensitivity enhancement of potassium ion (K⁺) detection based on graphene field-effect transistors with surface plasma pretreatment, *Sensor. Actuator. B Chem.* 285 (2019) 333–340.
- [36] R. Wang, Y. Mao, L. Wang, H. Qu, Y. Chen, L. Zheng, Solution-gated graphene transistor based sensor for histamine detection with gold nanoparticles decorated graphene and multi-walled carbon nanotube functionalized gate electrodes, *Food Chem.* 347 (2021) 128980.
- [37] S. Xu, J. Zhan, B. Man, S. Jiang, W. Yue, S. Gao, et al., Real-time reliable determination of binding kinetics of DNA hybridization using a multi-channel graphene biosensor, *Nat. Commun.* 8 (2017) 14902.
- [38] S.-K. Hu, F.-Y. Lo, C.-C. Hsieh, L. Chao, Sensing ability and formation criterion of fluid supported lipid bilayer coated graphene field-effect transistors, *ACS Sens.* 4 (2019) 892–899.
- [39] X. Wang, Y. Zhu, T.R. Olsen, N. Sun, W. Zhang, R. Pei, et al., A graphene aptasensor for biomarker detection in human serum, *Electrochim. Acta* 290 (2018) 356–363.
- [40] S.J. Park, S.E. Seo, K.H. Kim, S.H. Lee, J. Kim, S. Ha, et al., Real-time monitoring of geosmin based on an aptamer-conjugated graphene field-effect transistor, *Biosens. Bioelectron.* 174 (2021) 112804.
- [41] S. Chen, Y. Sun, Y. Xia, K. Lv, B. Man, C. Yang, Donor effect dominated molybdenum disulfide/graphene nanostructure-based field-effect transistor for ultrasensitive DNA detection, *Biosens. Bioelectron.* 156 (2020) 112128.
- [42] L. Qiang, Y. Zhang, C. Wu, Y. Han, S. Wang, Y. Wang, et al., A facile and sensitive DNA sensing of harmful algal blooms based on graphene oxide nanosheets, *Mar. Biotechnol.* 22 (2020) 498–510.
- [43] M.H. Rümmele, S. Gorantla, A. Bachmatiuk, J. Phielers, N. Geißler, I. Ibrahim, et al., On the role of vapor trapping for chemical vapor deposition (CVD), *Grown Graphene over Copper* 25 (2013) 4861–4866.
- [44] J. Pang, A. Bachmatiuk, L. Fu, C. Yan, M. Zeng, J. Wang, et al., Oxidation as a means to remove surface contaminants on Cu foil prior to graphene growth by chemical vapor deposition, *J. Phys. Chem. C* 119 (2015) 13363–13368.
- [45] D. Xiaochen, S. Yumeng, H. Wei, C. Peng, L.J.A.M. Lain-Jong, et al., Electrical detection of DNA hybridization with single-base specificity using transistors based on CVD-grown graphene sheets, 22, 2010, pp. 1649–1653.
- [46] C.T. Lin, L. Ptk, T.Y. Chen, K.K. Liu, C.H. Chen, K.H. Wei, et al., Label-free electrical detection of DNA hybridization on graphene using Hall effect measurements, *Revisiting the Sensing Mechanism* 23 (2013) 2301–2307.
- [47] X. Xu, C. Liu, Z. Sun, T. Cao, Z. Zhang, E. Wang, et al., Interfacial engineering in graphene bandgap, *ChSRv* 47 (2018) 3059–3099.
- [48] A. Lopez, J. Liu, Covalent and noncovalent functionalization of graphene oxide with DNA for smart sensing, *Advanced Intelligent Systems* 2 (2020) 2000123.
- [49] M. Yankowitz, Q. Ma, P. Jarillo-Herrero, B.J. LeRoy, van der Waals heterostructures combining graphene and hexagonal boron nitride, *Nat. Rev. Phys.* 1 (2019) 112–125.
- [50] S. Sheibani, L. Capua, S. Kamaei, S.S.A. Akbari, J. Zhang, H. Guerin, et al., Extended gate field-effect-transistor for sensing cortisol stress hormone, *Comm. Mater.* 2 (2021) 10.
- [51] R. Nieman, A.J.A. Aquino, H. Lischka, Exploration of graphene defect reactivity toward a hydrogen radical utilizing a preactivated circumcoronene model, *J. Phys. Chem.* 125 (2021) 1152–1165.
- [52] Y. Yan, D. Zhai, Y. Liu, J. Gong, J. Chen, P. Zan, et al., van der Waals heterojunction between a bottom-up grown doped graphene quantum dot and graphene for photoelectrochemical water splitting, *ACS Nano* 14 (2020) 1185–1195.
- [53] W. Haomin, W. Yihong, C. Chunxiao, S. Jingzhi, Y.J.A.N. Ting, in: Hysteresis of electronic transport in graphene transistors 4, 2010, pp. 7221–7228.
- [54] M. Bartošik, J. Mach, J. Piastek, D. Nežval, M. Konečný, V. Svarc, et al., Mechanism and suppression of physisorbed-water-caused hysteresis in graphene FET sensors, *ACS Sens.* 5 (2020) 2940–2949.
- [55] J. Gao, Y. Gao, Y. Han, J. Pang, C. Wang, Y. Wang, et al., Ultrasensitive label-free miRNA sensing based on a flexible graphene field-effect transistor without functionalization, *ACS Appl. Elect. Mater.* 2 (2020) 1090–1098.
- [56] J. Pena-Bahamonde, H.N. Nguyen, S.K. Fanourakis, D.F. Rodrigues, Recent advances in graphene-based biosensor technology with applications in life sciences, *J. Nanobiotechnol.* 16 (2018) 75.
- [57] S.S. Sekhon, P. Kaur, Y.-H. Kim, S.S. Sekhon, 2D graphene oxide–aptamer conjugate materials for cancer diagnosis, *npj 2D Mater. Appl.* 5 (2021) 21.
- [58] C. Wang, Y. Zhang, W. Tang, C. Wang, Y. Han, L. Qiang, et al., Ultrasensitive, high-throughput and multiple cancer biomarkers simultaneous detection in serum based on graphene oxide quantum dots integrated microfluidic biosensing platform, *Anal. Chim. Acta* 1178 (2021) 338791.
- [59] B. Liu, S. Salgado, V. Maheshwari, J. Liu, DNA adsorbed on graphene and graphene oxide: fundamental interactions, desorption and applications, *Curr. Opin. Colloid Interface Sci.* 26 (2016) 41–49.
- [60] D. Lee, W.H. Jung, S. Lee, E.-S. Yu, T. Lee, J.H. Kim, et al., Ionic contrast across a lipid membrane for Debye length extension: towards an ultimate bioelectronic transducer, *Nat. Commun.* 12 (2021) 3741.
- [61] V. Kesler, B. Murmann, H.T. Soh, Going beyond the Debye length: overcoming charge screening limitations in next-generation bioelectronic sensors, *ACS Nano* 14 (2020) 16194–16201.
- [62] J. Ping, J. Xi, J.G. Saven, R. Liu, A.T.C. Johnson, Quantifying the effect of ionic screening with protein-decorated graphene transistors, *Biosens. Bioelectron.* 89 (2017) 689–692.
- [63] W. Fu, L. Jiang, E.P. van Geest, L.M.C. Lima, G.F. Schneider, Sensing at the surface of graphene field-effect transistors, *Adv. Mater.* 29 (2017) 1603610.